microbial biotechnology

Open Access

SARS-CoV-2 RNA screening in routine pathology specimens

Saskia vonStillfried,[1,†] Sophia Villwock,[1,†] Roman D. Bülow,[1] Sonja Djudjaj,[1] Eva M. Buhl,[1,2] Angela Maurer,[1] Nadina Ortiz-Brüchle,[1] Peter Celec,[3,4,5] Barbara M. Klinkhammer,[1] Dickson W.L. Wong,[1] Claudio Cacchi,[1] Till Braunschweig,[1] Ruth Knüchel-Clarke,[1] Edgar Dahl[1,6,†] and Peter Boor[1,2,7,8,*,†]

[1]*Institute of Pathology, RWTH Aachen University Hospital, Aachen, Germany.*
[2]*Electron Microscopy Facility, RWTH Aachen University Hospital, Aachen, Germany.*
[3]*Institute of Virology, Biomedical Research Center, Slovak Academy of Sciences, Bratislava, Slovakia.*
[4]*Institute of Pathophysiology, Faculty of Medicine, Comenius University, Bratislava, Slovakia.*
[5]*Department of Molecular Biology, Faculty of Natural Sciences, Comenius University, Bratislava, Slovakia.*
[6]*RWTH Centralized Biomaterial Bank (RWTH cBMB), RWTH Aachen University Hospital, Aachen, Germany.*
[7]*Department of Nephrology, RWTH Aachen University Hospital, Aachen, Germany.*
[8]*Department of Immunology, RWTH Aachen University Hospital, Aachen, Germany.*

Summary

Virus detection methods are important to cope with the SARS-CoV-2 pandemics. Apart from the lung, SARS-CoV-2 was detected in multiple organs in severe cases. Less is known on organ tropism in patients developing mild or no symptoms, and some of such patients might be missed in symptom-indicated swab testing. Here, we tested and validated several approaches and selected the most reliable RT-PCR protocol for the detection of SARS-CoV-2 RNA in patients' routine diagnostic formalin-fixed and paraffin-embedded (FFPE) specimens available in pathology, to assess (i) organ tropism in samples from COVID-19-positive patients, (ii) unrecognized cases in selected tissues from negative or not-tested patients during a pandemic peak, and (iii) retrospectively, pre-pandemic lung samples. We identified SARS-CoV-2 RNA in seven samples from confirmed COVID-19 patients, in two gastric biopsies, one small bowel and one colon resection, one lung biopsy, one pleural resection and one pleural effusion specimen, while all other specimens were negative. In the pandemic peak cohort, we identified one previously unrecognized COVID-19 case in tonsillectomy samples. All pre-pandemic lung samples were negative. In conclusion, SARS-CoV-2 RNA detection in FFPE pathology specimens can potentially improve surveillance of COVID-19, allow retrospective studies, and advance our understanding of SARS-CoV-2 organ tropism and effects.

Received 3 January, 2021; accepted 27 April, 2021.
*For correspondence. E-mail pboor@ukaachen.de; Tel. +49 241 80 89280; Fax +49 241 80 82446.
[†][†]These authors contributed equally to this work.
Microbial Biotechnology (2021) **14**(4), 1627–1641
doi:10.1111/1751-7915.13828

Funding Information

This work was supported by the German Registry of COVID-19 Autopsies (www.DeRegCOVID.ukaachen.de), funded by the Federal Ministry of Health (ZMVI1-2520COR201), by the Federal Ministry of Education and Research within the framework of the network of university medicine (DEFEAT PANDEMIcs, 01KX2021 and STOP-FSGS-01GM1901A), the German Research Foundation (DFG; SFB/TRR57 – Project ID 36842431, SFB/TRR219 – Project-ID 322900939, BO3755/3-1, BO3755/9-1 – Project-ID 432698239, and BO3755/13-1 – Project-ID 454024652), and the RWTH START-Program (125/17).

Introduction

Identification and isolation of infected individuals with severe acute respiratory syndrome coronavirus-2 (SARS-CoV-2) is an effective preventive measure to limit the 2019 coronavirus disease (COVID-19) pandemic. Previous studies suggested that 40–45% of patients infected with SARS-CoV-2 develop only mild symptoms or even remain asymptomatic (Oran and Topol, 2020). Some patients may initially present with very mild respiratory or atypical, e.g., gastrointestinal, symptoms (Wang *et al*., 2020). This could limit the effectiveness in identifying infected individuals if the examination is indicated only by the presence of symptoms. Apart from the nasal and respiratory tract and the lung (Hou *et al*., 2020), several organs have been described as positive for viral RNA, especially the salivary gland, heart, liver, central nervous system, kidneys, lymph nodes, spleen and colon (Azzi *et al*., 2020; Lamers *et al*., 2020; Puelles *et al*., 2020; Sekulic *et al*., 2020).

Pathologists analyse a wide variety of samples from virtually all tissues, most of which are formalin-fixed and paraffin-embedded (FFPE). The latter is an efficient

method for long-term preservation of proteins and nucleic acids but also inactivates infectious agents, including SARS-CoV-2. Therefore, the analysis of FFPE specimens does not demand the high biosafety precautions required for swabs or unfixed specimens. A smaller proportion of specimens analysed in pathology, particularly for perioperative diagnostics, biobanking and some cytologic analyses, are processed unfixed and are thus potentially infectious (Guerini-Rocco *et al.*, 2020). To date, the majority of SARS-CoV-2 RNA analyses have been performed on FFPE autopsy specimens or cell pellets (Guerini-Rocco *et al.*, 2020; Lean *et al.*, 2020; Liu *et al.*, 2020; Puelles *et al.*, 2020). For the detection of SARS-CoV-2 in non-autopsy tissues, mainly case reports on a small number of individual patients and very few studies with more than 20 cases focusing on single organs have been published so far (Escher *et al.*, 2020; Smithgall *et al.*, 2020). In this single-centre study, we established a SARS-CoV-2 RNA detection protocol for FFPE material to (i) assess the feasibility of detecting viral RNA in samples from clinically diagnosed COVID-19 patients, (ii) evaluate the potential use of FFPE samples to screen for previously unrecognized infected patients, and (iii) consider the use of archival material, e.g. to screen for potential cases before identification of the first local index patients, as recently proposed (Deslandes *et al.*, 2020). To search for previously unrecognized infected patients, given the previous data on the traceability of SARS-CoV-2 RNA in various tissues and organs, we focused on samples from oropharyngeal and sinonasal mucosa, salivary glands, lung, colon and kidney (Borczuk *et al.*, 2020; Guerini-Rocco *et al.*, 2020; Puelles *et al.*, 2020; Remmelink *et al.*, 2020; Sekulic *et al.*, 2020).

One of the first and most affected SARS-CoV-2 hotspots in Germany was in the catchment area of our centre in Aachen, with 22% asymptomatic patients (Streeck *et al.*, 2020). Therefore, our Institute of Pathology was well positioned to address the above research questions using FFPE material from our diagnostic archive.

Results

Evaluation of two RNA isolation systems and RT-PCR SARS-CoV-2 RNA detection systems for FFPE specimen screening

Since tissue processing of FFPE specimens may influence RNA quality and quantity, we tested two different isolation systems for RNA isolation, i.e. automated magnetic particle purification and manual spin-column purification. The yield of total RNA was comparable for both methods (Fig. S1a). The RNA quality showed a strongly degraded RNA after isolation with both methods (Fig. S1b and c). However, viral SARS-CoV-2 RNA could be detected in all assessed positive samples (viral copy numbers of 8 to 12 000 μl^{-1}) independently of the RNA isolation method used (Fig. S1d and e). For further sample processing, we used automated magnetic particle purification.

Using a SARS-CoV-2 RNA standard with a defined viral copy number (twofold dilution), we validated two different one-step RT-PCR methods (TaqMan and RealStar) in single- and multiplex approaches with different primer and probe sets for SARS-CoV-2 RNA detection (Fig. 1A), and evaluated RNA detection in FFPE samples in this context. Using the TaqMan method, we analysed the RT-PCR efficiencies of the SARS-CoV-2 E gene, the RdRp gene and the N gene as previously suggested (Corman *et al.*, 2020), in a singleplex approach for selecting two assays to establish a dual-target assay. We found that only the E gene assay was within the range of efficient RT-PCR, and the RdRp and N gene assay were out of range ($>$ 110%). The RdRp-gene assay had been suggested previously as a confirmatory test (Corman *et al.*, 2020). Therefore, we additionally analysed the RT-PCR efficiency of the E and RdRp gene in a multiplex approach as a potential method to save resources, but we found that the efficiency was impaired in the multiplex approach (Fig. 1B). The RealStar method is a simple single-tube assay that detects the SARS-CoV-2 S gene and the B-βCoV E gene in a multiplex approach as a dual-target assay. We measured amplification and, using linear regression, found that RT-PCR efficiency for the SARS-CoV-2 S gene and the B-β-CoV E gene were within the range of efficient RT-PCR (90–110%) (Taylor *et al.*, 2010). We have compared the TaqMan singleplex and multiplex method of the E gene and RdRp gene by the Bland–Altman plot, showing the bias for both is close to zero, indicating no systematically different results. In general, we observed higher Ct values (1–3.5 C_t values) for detection of the RdRp gene in the SARS-CoV-2 RNA standard dilution compared to detection of the E gene at the same viral copy number. Based on the linearity of the SARS-CoV-2 RNA standard dilution series, we additionally determined the limit of detection (LOD) within a 95% confidence interval as viral copy number μl^{-1}. Comparing the TaqMan singleplex to multiplex approach, we found that the LOD for both the E and the RdRp genes decreased from the singleplex to the multiplex approach (E gene: 7 to 14 viral copy numbers μl^{-1}, RdRp gene 14 to 27 viral copy numbers μl^{-1}). For the TaqMan singleplex approach of the N gene, we found that the LOD was even lower (55 viral copy numbers μl^{-1}) than the LOD of the E and RdRp genes. The LOD of the RealStar multiplex approach was in the same range as the LOD of the singleplex approach of the E and RdRp genes (SARS-CoV-2 S gene: 14 viral copy numbers μl^{-1}, B-βCoV E gene: 7 viral copy numbers μl^{-1}, Table 1). To evaluate RT-PCR methods in

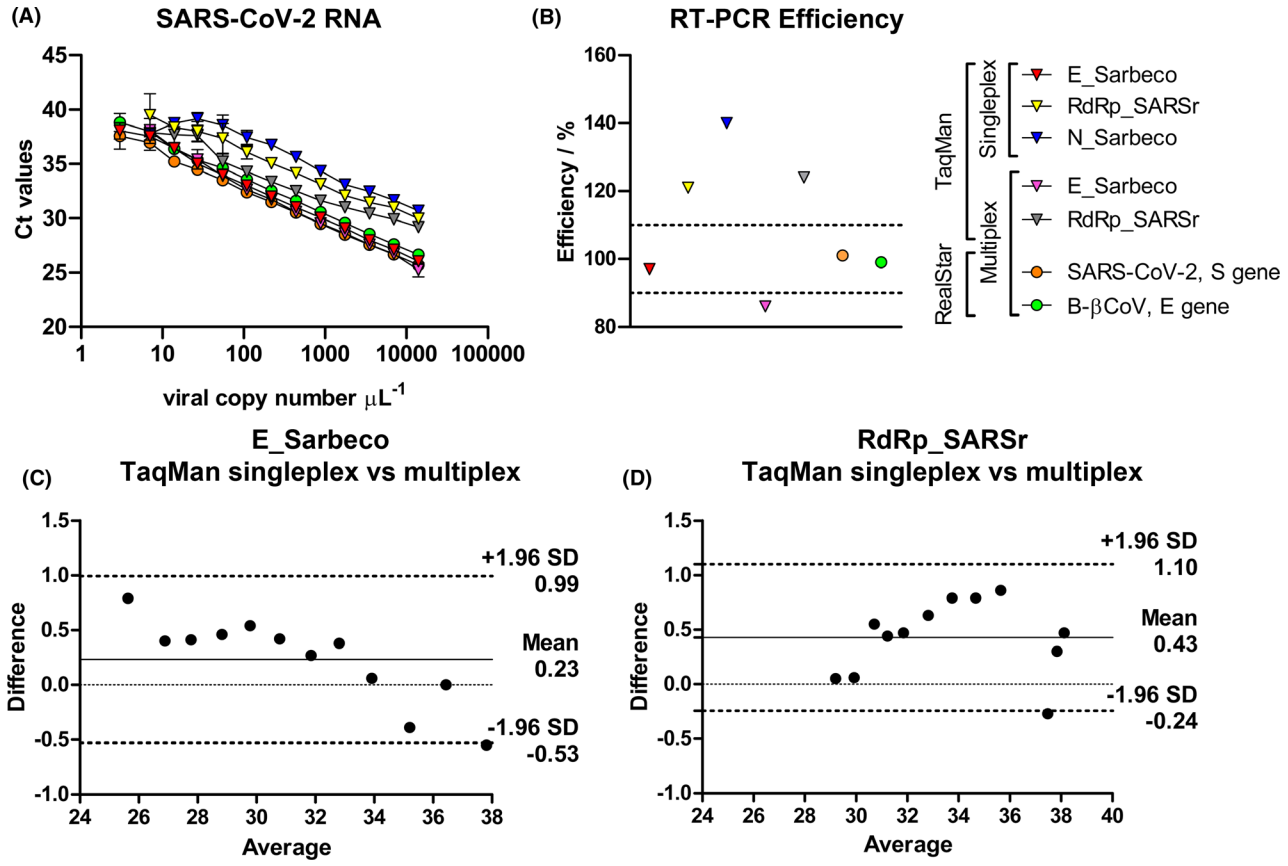

Fig. 1. Evaluation of RT-PCR efficiency of the different primer and probe sets with the two different RT-PCR methods by SARS-CoV-2 RNA standard. (A) C_t values of primer and probe sets as singleplex and multiplex approaches using TaqMan and RealStar methods in twofold dilution series of SARS-CoV-2 RNA standard. (B) Using linear regression of each assay, RT-PCR efficiency was calculated according to the equation $100\times\ (-1 + 10^{-1/\text{slope}})$. For successful RT-PCR assays, the efficiency ranges from 90 to 110% (dotted lines, Taylor *et al*., 2010). Bland–Altman plots for comparison of TaqMan singleplex and multiplex methods for the targets (C) E_Sarbeco and (D) RdRp_SARSr show a mean bias close to zero, indicating a low average discrepancy.

FFPE samples, we used diluted RNA (1:50) isolated from the trachea and lung samples of clinically confirmed COVID-19 autopsy cases. Because of the good RT-PCR efficiency results, we compared the TaqMan singleplex approach and RealStar multiplex approach for the E gene assay, and found that in the same samples, SARS-CoV-2 RNA detection was positive with the TaqMan method but negative with the RealStar method (Table 2). Therefore, we established a workflow for SARS-CoV-2 RNA detection using the TaqMan RT-PCR singleplex approach with the E gene assay for screening RNA isolated from FFPE tissue samples from patients. For confirmatory testing (dual-target assay), we established the RdRp gene assay (Fig. S2).

Detection of SARS-CoV-2 RNA in the COVID-19 patients cohort

In the COVID-19-positive patient cohort, the relatively small number of tissue samples ($n = 47$ samples from 34 patients, Table S1) was not surprising because invasive procedures are kept to a minimum in COVID-19 patients. The 47 samples included seven specimens in which SARS-CoV-2 RNA was detectable (two gastric biopsy specimens, one small bowel resection specimen and one colon resection specimen, one pleural resection specimen, one lung specimen and one FFPE specimen from a cytospin preparation of a pleural effusion (Fig. 2A and D; patient 23, Table 4)). Using fluorescence *in situ* hybridization (FISH), intracytoplasmic SARS-CoV-2 RNA was detectable in cells morphologically identified as macrophages in the pleural effusion sample (Fig. 2B′), supported by hematoxylin-eosin staining (Fig. 2C′). This sample, as well as autopsy lung samples from COVID-19 patients (Fig. 2B‴, C‴, D), allowed us to confirm the specificity of the RT-PCR method with an independent FISH approach using a different target RNA sequence.

In patients with mild disease progression (i.e. not requiring mechanical ventilation, Table 3) and earlier COVID-19 stage (i.e. < 14 days after first symptoms/

Table 1. Detection of SARS-CoV-2 in RNA standard dilution series by the various RT-PCR methods.

Method	TaqMan singleplex			TaqMan singleplex			TaqMan singleplex			TaqMan multiplex						RealStar multiplex					
	E gene Ct SARS-CoV-2			RdRp gene Ct SARS-CoV-2			N gene Ct SARS-CoV-2			E gene Ct SARS-CoV-2			RdRp gene Ct SARS-CoV-2			S gene Ct SARS-CoV-2			E gene Ct B-ßCoV		
Copy number	Mean	SD	*n*	Mean	SD	*n*	Mean	SD	*n*	Mean	SD	*n*	Mean	SD	*n*	Mean	SD	*n*	Mean	SD	*n*
14000	26.03	0.075	5	29.22	0.090	5	30.69	0.194	5	25.24	0.563	5	29.17	0.033	5	25.67	0.067	5	26.64	0.044	5
7000	27.09	0.042	5	29.95	0.088	5	31.66	0.199	5	26.69	0.043	5	29.89	0.099	5	26.65	0.064	5	27.59	0.053	5
3500	27.98	0.102	5	30.98	0.077	5	32.45	0.206	5	27.57	0.046	5	30.43	0.086	5	27.54	0.027	5	28.53	0.062	5
1750	29.06	0.084	5	31.44	0.149	5	33.10	0.083	5	28.60	0.069	5	31.00	0.043	5	28.49	0.050	5	29.57	0.073	5
875	30.05	0.080	5	32.08	0.141	5	34.35	0.265	5	29.51	0.080	5	31.61	0.151	5	29.48	0.044	5	30.55	0.103	5
438	31.00	0.138	5	33.13	0.128	5	35.63	0.307	5	30.58	0.081	5	32.50	0.170	5	30.52	0.055	5	31.58	0.074	5
219	31.99	0.137	5	34.14	0.089	5	36.76	0.224	5	31.72	0.136	5	33.35	0.173	5	31.49	0.104	5	32.52	0.070	5
109	33.00	0.057	5	35.06	0.128	5	37.44	0.577	5	32.62	0.084	5	34.27	0.274	5	32.38	0.051	5	33.55	0.170	5
55	33.95	0.129	5	36.07	0.556	5	38.55	0.826	5	33.89	0.149	5	35.21	0.621	5	33.49	0.078	5	34.62	0.167	5
27	35.01	0.284	5	37.34	1.219	5	39.14	0.508	4	35.40	0.806	5	37.61	0.522	5	34.47	0.287	5	35.36	0.197	5
14	36.44	0.385	5	37.99	0.806	5	38.76	0.316	2	36.44	0.293	5	37.69	0.630	4	35.21	0.347	5	36.37	0.349	5
7	37.54	0.589	5	38.35	0.092	4	37.76	0.393	2	38.09	–	1	37.88	-	1	36.95	0.608	4	37.99	1.064	5
3	38.04	0.647	4	39.48	1.615	3	*ND*	–	*0*	*ND*	–	*0*	*ND*	–	0	37.55	1.036	4	38.81	0.715	4

C_t values for SARS-CoV-2 RNA detection using TaqMan singleplex (E, RdRp, and N gene), TaqMan multiplex (E, RdRp gene) and RealStar multiplex (S gene, E gene B-ßCoV) assays in two-fold SARS-CoV-2 RNA standard dilutions with defined copy numbers. Only TaqMan singleplex E and RdRp gene and RealStar multiplex assays have high LODs with 7–14 viral copy numbers μl^{-1} (n = number of detectable values in five replicate measurements). ND, not detectable.

Table 2. SARS-CoV-2 RNA detection in FFPE tissues.

		TaqMan Singleplex			RealStar Multiplex		
Tissue	Dilution	pos./neg.	Ct-SARS-CoV-2 E gene	Viral copy number μl^{-1}	pos./neg.	Ct-SARS-CoV-2 S gene	Ct-B-ßCoV E gene
Trachea	1:50	Positive	34.50	43	Negative	ND	ND
Lung	1:50	Positive	34.88	33	Negative	ND	ND
Lung	1:50	Positive	34.45	4429	Negative	ND	ND

Isolated and diluted (1:50) RNAs from FFPE tissue (trachea, lung) from clinically confirmed COVID-19 autopsy cases were positive at 33–44 viral copy numbers μl^{-1} in the TaqMan singleplex (E gene) approach, but negative for SARS-CoV-2 in the RealStar multiplex approach.

test), SARS-CoV-2 RNA was found in two gastric biopsies (patients 5 and 6, Table 3), but was not detectable in soft tissues, normal and neoplastic oral mucosa, lymph nodes, salivary gland, ovarian and peritoneal lavage fluid and placenta (Table 3). In patients with mild disease in later COVID-19 stages (> 14 days after first symptoms/test), SARS-CoV-2 RNA was detectable in a pleural resection specimen from a patient 48 days after the first positive test (patient 13, Table 3), while other samples, including pleural effusion from the same patient (patient 13, Table 3), pulmonary tissues, lymph node, liver and colon, were negative.

In patients with severe disease (i.e. requiring mechanical ventilation, Table 4) in early COVID-19 (< 14 days after first symptoms/test), samples from pleural effusion (patient 23, Table 4) and small bowel (patient 24, Table 4) were positive for SARS-CoV-2 RNA, while soft tissue was negative. In later COVID-19 stages (> 14 days after first symptoms/test) in severe disease courses, one large bowel sample was positive (patient 32, Table 4), while other samples from small and large bowel, thymus neoplasia, bone marrow and one pleural effusion were negative for SARS-CoV-2 RNA. Morphologically, no characteristic features of viral infection or sequelae of viral infection were evident in extrapulmonary tissues.

Lung samples from three patients with onset of COVID-19 symptoms long before surgery, i.e. 50–81 days, showed pulmonary morphologies consistent with the severity of clinical COVID-19 disease progression, e.g. focal fibrosis in a mild disease course (patient 14, Table 3, Fig. 3A′ and A′′) and diffuse fibrosis with nearly complete obliteration of the alveolar spaces in severe disease courses (patient 29, Table 4, Fig. 3B′ and B′′). In one patient, a pulmonary biopsy 76 days after the first symptoms was still positive for SARS-CoV-2 RNA (patient 15, Table 3). Morphologically, the biopsy showed pulmonary fibrosis. Confounding factors such as previous lung disease, radiation to the lungs or a history of tobacco abuse were not known to exist in these patients.

SARS-CoV-2 detection in the pandemic peak cohort

SARS-CoV-2 RNA was detected in two samples from the pandemic peak period in a previously unrecognized COVID-19 patient (Fig. 2A). The positive samples were bilateral tonsillectomy specimens from a female patient in her twenties with clinical symptoms of tonsillitis and peritonsillar abscess formation (139–169 viral copies μl^{-1}, Fig. 2B'', C'' and D). She remained without symptoms typical for COVID-19. The remaining $N = 221$ specimens from the head and neck, colon, lung and kidney during the pandemic peak were negative (Tables S2 and S3).

SARS-CoV-2 detection in the pre-pandemic cohort showed no positive cases

None of the $N = 93$ samples in the pre-pandemic cohort were positive for SARS-CoV-2 RNA (Fig. 2A, Table S4).

Discussion

This study established and validated SARS-CoV-2 RNA detection methods in non-autopsy FFPE tissues, showing its utility as a prospective and retrospective screening method and a tool to investigate organ tropism and effects of SARS-CoV-2. The RNA extraction is a bottleneck during PCR for SARS-CoV-2, and the availability of extraction kits may be limited during a pandemic. Therefore, we tested two different RNA extraction methods on clinically confirmed SARS-CoV-2-positive autopsy FFPE tissues. Our data suggested that the performance is not dependent on the RNA isolation method, and the results are consistent even in highly degraded RNA. For RT-PCR, we used commercially available kits that enable broad applicability, and validated the analytical efficiency and limit of detection, as suggested previously (Forootan *et al*., 2017; Vogels *et al*., 2020). We established a dual-target assay using the E gene assay (TaqMan) as first-line screening and the RdRp gene assay (TaqMan) as a confirmatory test; both assays in a singleplex approach

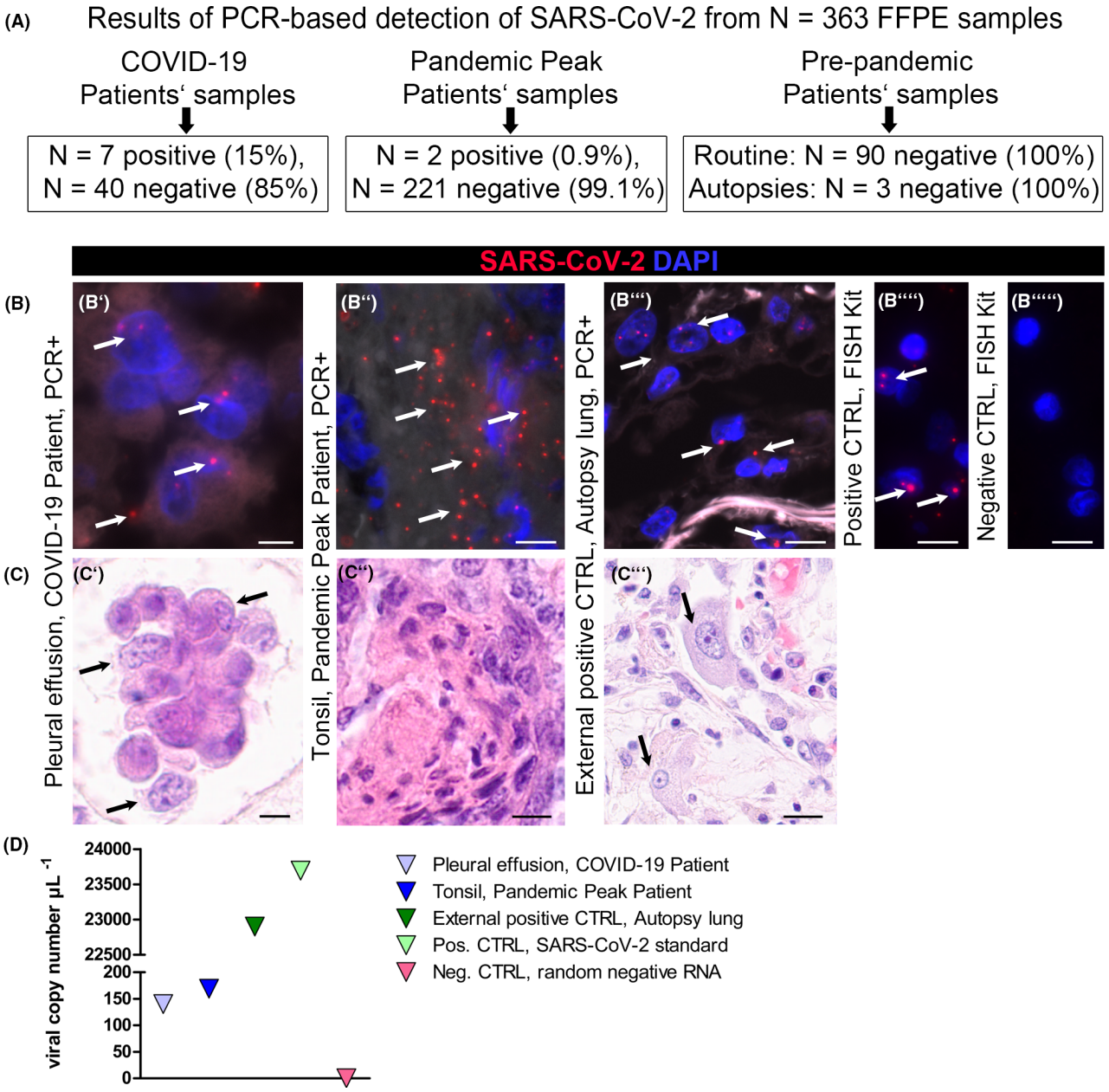

Fig. 2. Results of RT-PCR-based detection of SARS-CoV-2 RNA in the three cohorts studied (N = 363) and method validation using fluorescence in situ hybridization (FISH). (A) SARS-CoV-2 RT-PCR detection in all three cohorts resulted in four positive samples in COVID-19 patient samples and one positive sample in pandemic peak patient samples. (B–C) Method validation by FISH and hematoxylin-eosin staining; (B') SARS-CoV-2 RNA-positive pleural effusion sample (arrows, patient 12, Table 4) and (B'') SARS-CoV-2-positive tonsil sample from pandemic patient with viral RNA in detritus-filled crypts (arrows); (B''') lung tissue from an autopsy case with clinically confirmed SARS-CoV-2 infection showed a red fluorescent signal of SARS-CoV-2 RNA (arrows, scale bar = 5 µm), (B'''') positive control with a red fluorescent signal of Homo sapiens POLR2A gene (arrows, scale bar = 10 µm), (B''''') Negative control (dap gene from Bacillus subtilis, scale bar = 10 µm). (C') Light micrograph of pleural effusion sample showing a group of reactive macrophages (arrow, HE, scale bar = 10 µm). (C'') Light micrograph of tonsil sample in (B''); (C''') light micrograph of lung tissue in (B''') with reactive macrophages (arrows, HE, scale bar = 20 µm). (d) RT-PCR results (individual SARS-CoV-2 E-gene viral copy number μl^{-1}) of the samples.

are in line with a previous study (Corman *et al.*, 2020). A dual-target assay is included in most commercially available molecular diagnostic kits for SARS-CoV-2 RNA detection to increase sensitivity and specificity, but single-target assays are also available (Afzal, 2020). Our results show typical analytical RT-PCR efficiencies for the target E gene assay, and the detection limit of the RdRp gene was higher than that of the E gene. When

Table 3. Patient characteristics of COVID-19-Positive Patients with mild disease course.

Patient No.	Sex	Age range	Duration of ventilation (d)/ hospitalization (d)	First symptoms (d +/- sampling)	Positive test for SARS-CoV-2 (d +/- sampling; localization) First	Last	SARS-CoV-2 RNA from FFPE	Viral copy number/ µl	Localization	Indication for surgery/sampling	Specimen received as	Histologic result
Mild disease course without mechanical ventilation												
1[a]	M	76–80	0/1	Unknown	Unknown		neg	.	Appendix	Appendicitis	Formalin-fixed resection	Appendix with acute serositis
2[b]	F	81–85	0/27	Asymptomatic	7; upper airways	18; upper airways	neg	.	Right kidney	Neoplasia	Formalin-fixed resection	Urothelial cancer
3[b]	M	61–65	0/18	3	3; upper airways		neg	.	Left lateral oral floor	Neoplasia	PERIOPERATIVE fresh-frozen section	Tumour-free oral mucosa
							neg	.	Anterior oral floor		Formalin-fixed resection	SCC of oral mucosa
							neg	.	Left lymph node level IIa		Perioperative fresh-frozen section	Lymph node
							neg	.	Right lymph node level IIa		Perioperative fresh-frozen section	
							neg	.	Left submandibular gland		Perioperative fresh-frozen section	
		Salivary gland										
4[b]	F	31–35	0/1	Asymptomatic	0; upper airways		neg	.	Right ovary	Neoplasia	Perioperative fresh-frozen section	Borderline tumour of ovary
								.	Left ovary		Formalin-fixed resection	
								.	Peritoneal cavity		Peritoneal lavage fluid	
5[b]	M	71–75	0/9	Unknown	1; upper airways		**pos**	6	Gastric antrum	Gastritis	Formalin-fixed biopsy	Chronic antrum gastritis, no intestinal metaplasia, no helicobacter pylori
6[b]	M	51–55	0/18	Asymptomatic	−1; upper airways		**pos**	1693	Gastric antrum	Gastritis	Formalin-fixed biopsy	Chronic antrum gastritis, intestinal metaplasia, no helicobacter pylori

Table 3. (Continued)

Patient No.	Sex	Age range	Duration of ventilation (d)/ hospitalization (d)	First symptoms (d +/- sampling)	Positive test for SARS-CoV-2 (d +/- sampling; localization)		SARS-CoV-2 RNA from FFPE	Viral copy number/ µl	Localization	Indication for surgery/sampling	Specimen received as	Histologic result
					First	Last						
7[b]	F	31–35	0/2	Asymptomatic	−1; upper airways		neg	.	Uterine cavity	Missed abortion	Formalin-fixed resection	Placenta and endometrium
8[b]	M	5–15	0/11	Asymptomatic	−5; upper airways	1; upper airways	neg	.	Peritoneal cavity	Ascites	Cytology	Mesothelia, macrophages
9[b]	F	66–70	0/26	Asymptomatic	−11; upper airways		neg	.	Left upper thigh soft tissue	Impaired wound healing	Formalin-fixed resection	Soft tissue with low-grade inflammation
10[b]	M	76–80	0/18	−21	−18; upper airways	4; upper airways	neg	.	Upper left lung lobe bronchus mucosa	Mediastinal nodule	Formalin-fixed resection	Inflammatory bronchial and peribronchial tissue
11[b]	M	56–60	0/8	−21	−21; upper airways		neg	.	Coecum	Change in bowel habit	Formalin-fixed biopsy	Ulceration
12[b]	M	66–70	0/68	−30	−29; upper airways		neg	.	Left and right liver lobe	Transplant	Formalin-fixed resection	Liver cirrhosis
13[b]	M	41–45	Unknown	Unknown	−48; unknown	−45; unknown	neg	.	Pleural effusion	Pleural empyema	Ethanol-fixed cytology	Granulocytes, mesothelia, macrophages
							pos	4	Pleural tissue		Formalin-fixed resection	Pleuritis
14[b]	M	61–65	0/5	−66	−60; upper & lower airways		neg	.	Lingular lymph node	Neoplasia	Perioperative fresh-frozen section	Lymph node MET of RCC
							neg	.	Left lung lingula		Perioperative fresh-frozen section	Lung MET of RCC
							neg	.	Lower left lung lobe		Formalin-fixed resection	DAD, organizing with acute inflammation
15[b]	M	71–75	0/31	−76	−73; upper airways	Unknown	**pos**	2	Left lung lobe	Lung consolidation	Formalin-fixed biopsy	Lung fibrosis
16[b]	M	61–65	0/0	Asymptomatic	−228; upper airways		neg	.	Bronchial lavage	Lung fibrosis	Ethanol-fixed cytology	Respiratory epithelia, macrophages

Clinically confirmed COVID-19 patients with mild COVID-19 infection without mechanical ventilation. Time of surgery/sampling was set as zero, times are given as days -/+ = before/after surgery/sampling. DAD, diffuse alveolar damage; FFPE, formalin-fixed paraffin-embedded; MET, metastasis; RCC, renal cell carcinoma; SCC, squamous cell carcinoma.

a. Deceased.

b. Dismissed.

Table 4. Patient characteristics of COVID-19-Positive Patients with severe disease course.

Patient No	Sex	Age range	Duration of ventilation (d) / hospitalization (d)	ECMO (yes/no)	First symptoms (d +/- sampling)	Positive test for SARS-CoV-2 (d +/- sampling; localization)		SARS-CoV-2 RNA from FFPE	Viral copy number/µl	Localization	Indication for surgery/ sampling	Specimen received as	Histologic result
						First	Last						
Severe disease course without mechanical ventilation													
17 Unknown	M	66–70	Unknown	No	Unknown	Unknown		neg	.	Soft tissue	Necrosis	Formalin-fixed resection	Decubitus ulcer
18[b]	M	61–65	Unknown	No	Unknown	Unknown		neg	.	Pleural cavity	Pleural effusion	Ethanol-fixed cytology	Macrophages; mesothelia
19 Unknown	M	56–60	Unknown	No	Unknown	Unknown		neg	.	Left distal main bronchus and carina upper/lower left lung lobe	Bronchitis, tracheitis	Formalin-fixed biopsy	Bronchitis with squamous metaplasia
20[b]	M	56–60	3/18	No	Unknown	Unknown		neg	.	Pleural tissue	Pleural empyema	Formalin-fixed resection	Pleuritic
								neg	.	Pleural cavity	Pleural effusion	Ethanol-fixed cytology	Granulocytes, erythrocytes, fungi
21[a]	M	46–50	30/30	Yes	Unknown	−58; unknown		neg	.	Intrabronchial space	Endotracheal tube suction	Formalin-fixed biopsy	Necrotic material, fibrin
22[a]	F	66–70	12/33	No	1	1; upper airways		neg	.	Cubital joint	Exclusion of osteomyelitis	Formalin-fixed resection	Synovitis
23[a]	F	56–60	8/8	Yes	Unknown	−7; lower airways	−1; upper airways	**pos**	141	Pleural cavity	Pleural effusion	Ethanol-fixed cytology	Macrophages; mesothelia
24 [a]	F	51–55	14/14	No	−14	Unknown	−12; upper airways	**pos**	2	Small bowel	Ischemia	Formalin-fixed resection	Ischemic enteritis
25[a]	M	56–60	18/18	Yes	−21	−10; upper airways	1; lower airways	neg	.	Mediastinum	Neoplasia	Perioperative fresh-frozen section	Thymic neoplasia
					-22	-11; upper airways	0; lower airways	neg	.	mediastinum		Formalin-fixed resection	
26[a]	M	56–60	27/27	Yes	Unknown	−15; lower airways	0; lower airways	neg	.	Pleural cavity	Pleural effusion	Alcohol-fixed cytology	Macrophages; mesothelia
27a	M	71–75	12/21	No	−20	−20; upper airways	14; lower airways	neg	.	Ileum	Ischemia	Formalin-fixed resection	Ischemic enteritis
					−19	−19; upper airways	15; lower airways	neg	.	Colon ascendens			Ischemic colitis
28[a]	F	66–70	26/26	No	Unknown	−25; lower airways	−7; lower airways	neg	.	Colon transversum	Ischemia	Formalin-fixed resection	Ischemic colitis
29[b]	M	56–60	36/50	No	−50	−44; upper & lower airways		neg	.	Colon ascendens	Bleeding	Formalin-fixed resection	Ischemic colitis
						-47; upper & lower airways		neg	.	Upper right lung lobe	Lung nodules	Formalin-fixed resection	Haemorrhagic lung infarction

Table 4. (Continued)

Patient No	Sex	Age range	Duration of ventilation (d) / hospitalization (d)	ECMO (yes/no)	First symptoms (d +/- sampling)	Positive test for SARS-CoV-2 (d +/- sampling; localization)		SARS-CoV-2 RNA from FFPE	Viral copy number/µl	Localization	Indication for surgery/sampling	Specimen received as	Histologic result
						First	Last						
30[b]	M	26–30	61/75	Yes	Unknown	−53; lower airways	−36; upper airways	neg	.	Bone marrow iliac crest	Hemophagocytic lymphohistiocytosis	Formalin-fixed biopsy	Trilinear maturation, normocellular, abundant macrophages
31[b]	M	56–60	71/97	Yes	−60	−55; upper airways	−35; lower airways	neg	.	Colon sigmoideum	Diverticulitis	Formalin-fixed resection	Diverticulosis
32[a]	F	66–70	6/6	No	−60	−57; upper airways	0; upper airways	neg	.	Coecum	Peritonitis	Formalin-fixed resection	Colitis
								pos	7	Colon sigmoideum		Formalin-fixed resection	Colitis
33[a]	F	66–70	76/76	No	Unknown	−59; lower airways	−46; sputum	neg	.	Colon ascendens	Ulcus	Formalin-fixed biopsy	Hyperplastic colon mucosa
34[a]	M	46–50	82/83	Yes	−82	−81; upper airways	−46; lower airways	neg	.	Middle right lung lobe	Lung nodules	Formalin-fixed resection	Lung infarction

Clinically confirmed COVID-19 patients with severe COVID-19 infection on mechanical ventilation. Time of surgery/sampling was set as zero, times are given as days -/+ = before/after surgery/sampling. DAD, diffuse alveolar damage; ECMO, extracorporeal membrane oxygenation; FFPE, formalin-fixed paraffin-embedded.

a. Deceased.

b. Dismissed.

comparing the Ct values of the E and RdRp gene assays of the SARS-CoV-2 RNA standard dilution with each other, we found that the Ct values at the same viral copy number for the RdRp gene were generally higher than the Ct values of the E gene, indicating lower virus detection rates by the RdRp gene assay. A possible reason for this observation could be the detection of genomic and subgenomic RNA, since the RdRp gene is present only in genomic RNA (ORF1b) and the E gene is present in the genomic and also in subgenomic RNA (Alexandersen *et al*., 2020; Kim *et al*., 2020). Therefore, we used the linear regression of the standard SARS-CoV-2 RNA for the E gene to determine the viral load in samples. Previous studies attributed the lower virus detection to mismatch of the RdRp reverse primer and described the assay as not reliable for samples with < 1000 copy numbers μl^{-1} (Corman *et al*., 2020). In contrast, we found LOD at a viral copy number of 14 μl^{-1} using the RdRp gene assay. However, in the clinically confirmed COVID-19 patient cohort, we found seven positive samples using the detection of the E gene, two with a higher viral load (> 140 viral copies μl^{-1}) and five with a comparatively low viral load (< 7 viral copies μl^{-1}), whereas viral RNA from samples with low viral load was undetectable using the RdRp gene assay. This suggests that detection of the RdRp gene in RNA isolated from FFPE samples is less efficient compared to the SARS-CoV-2 RNA standard, but the RdRp gene can be detected up to at least 140 viral copies μl^{-1}. Taken together, our established SARS-CoV-2 RNA detection method provides a reliable screening method for RNA isolated from FFPE specimens.

The virus detection method can be used to analyse viral spread in different organs and disease mechanisms by correlating pathological and molecular findings with virus presence in specimens from previously confirmed COVID-19 patients. Previous studies in autopsies from deceased COVID-19 patients suggested that a low to very low viral load can be detected in extrapulmonary organs (Best Rocha *et al*., 2020; Menter *et al*., 2020; Polak *et al*., 2020; Puelles *et al*., 2020; Sekulic *et al*., 2020; Wichmann *et al*., 2020). However, these are all severe and fatal cases, and it remained unclear whether such viral spread is also found in less severe and non-fatal cases. For this, analyses of pathology specimens might likely be the only available approach. In four out of 16 patients (25%) with a mild disease course not requiring mechanical ventilation, we detected SARS-CoV-2 RNA in two gastric biopsies at a very early stage of infection (one day before and one day after the first positive swab, respectively) and in later stages in pleural and lung tissues (48–73 days after the first positive swab). Interestingly, we found the highest viral copy number of all positive samples in a gastric biopsy sample from an asymptomatic patient. To our knowledge, detection of viral RNA in gastric tissues has previously not been reported. This is likely because mostly post-mortem tissues were analysed previously, which are usually subject to strong autolytic changes in the stomach. We detected SARS-CoV-2 RNA in three out of 18 patients (17%) with a severe disease course requiring mechanical ventilation. We identified a SARS-CoV-2 RNA-positive FFPE sample from a pleural effusion cytospin preparation of a severely ill COVID-19 patient in the early phase of infection (< 14 days after first symptoms, patient 23). Because the sample contained predominantly macrophages, this suggests the presence of the virus in these cells. We confirmed and visualized this finding with direct detection of viral RNA by FISH in these cells, in agreement with previous reports showing SARS-CoV-2 RNA in pleural effusion fluid (Lescure *et al*., 2020; Mei *et al*., 2020). Finally, we found one positive small bowel sample in an earlier stage (14 days after first symptoms) and one colonic resection specimen, interestingly in a late stage 57 days after the first positive test, confirming previous reports of positive RNA detection in the colon and wastewaters (Lamers *et al*., 2020; Lodder and de Roda Husman, 2020; Remmelink *et al*., 2020).

Of the 15 PCR-negative samples from COVID-19 patients with severe symptoms, one patient was in an asymptomatic early phase of the disease (one day before the first symptoms), and eleven were in a later phase of the disease, i.e. > 14 days after the first symptoms. In the later phase of the disease, the virus was likely already eliminated from the organism by the immune system, and therefore was not detectable in other colon or lung samples. The negative SARS-CoV-2 RT-PCR of the lung samples, some of which showed progressive circumscribed or organized diffuse alveolar damage, suggests ongoing tissue damage in the absence of the virus and thereby might help to differentiate direct effects from sequelae of COVID-19. The data also confirm the concept of fibrotic pulmonary late effects of COVID-19 (Polak *et al*., 2020).

We investigated the feasibility of using pathology specimens to screen for SARS-CoV-2. We did this because (i) even during the first pandemic peak in our region, SARS-CoV-2 testing was only performed when patients were symptomatic, whereas some infections are known to be mild or even asymptomatic, (ii) false-negative results, especially depending on the stage of the disease, are not uncommon, (iii) no additional patient intervention is required to perform this test, (iv) in case of a positive result, improved tracing of infection would be possible, (v) in case of a positive result, additional and more complex molecular analyses on these tissues would be possible, e.g. cell-specific virus detection using

FISH. Compared to FISH, RT-PCR has the advantage of higher throughput, easier interpretation and much easier quantification. Therefore, we would recommend a sequential approach, screening samples with RT-PCR for the presence of SARS-CoV-2 RNA first, followed by the methods allowing the localization of the positive signal to specific cells using FISH (von Stillfried and Boor, 2021). For this analysis, we focused on periods of local pandemic peaks and on tissues that were most frequently positive for SARS-CoV-2 RNA in previous studies. Interestingly, among the $n = 223$ samples analysed, we found one previously unrecognized positive patient who underwent bilateral tonsillectomy. In addition to identifying new COVID-19 patients, this might also help to improve occupational hazard assessment for staff involved in specimen acquisition, e.g. in surgery, and processing, e.g. in pathology. The analysis of SARS-CoV-2 RNA can provide information on potential exposure to such unrecognized infectious specimens, which is particularly important in perioperative diagnostics, biobanking or cytology, where fresh unfixed specimens are processed directly.

Finally, this method also allows retrospective studies to be performed on archived FFPE material. A previous study reported a retrospective positive SARS-CoV-2 RNA detection in a respiratory specimen from December 2019 in France, well before the onset of the pandemic in Europe (Deslandes *et al*., 2020). In our cohort focusing on the most affected lung tissues, we did not find a single positive case between December 2019 and February 2020.

Limitations

The study has several limitations. These include the single-centre design and the relatively small sample size, especially for samples from COVID-19 confirmed patients. Despite this, our screening could identify a previously unrecognized case of COVID-19 and also indicated no viral spread beyond gastrointestinal tract, lungs and pleural cavity in mild COVID-19 cases. We believe that future larger and multicentre studies could further address these limitations, potentially in a similar approach to COVID-19 autopsies, for which we recently established a national registry aimed at collecting data from all COVID-19 autopsies in Germany to enable large-scale analyses (www.DeRegCOVID.ukaachen.de) (von Stillfried *et al*., 2020).

In COVID-19-positive patients, we did not have information on the date of first symptoms or the first test in five of the 34 cases, limiting the interpretation of these data. Another limitation is the overall reduced number of specimens sent for histopathologic analysis during the lockdown. Starting in calendar week 13 in 2020, all hospitals were asked to postpone all elective procedures to keep ICUs free for COVID-19 patients and minimize the risk of transmission to patients within the hospital. This was reflected in a 12% reduction in pathology specimens received at our centre compared with the same time in previous years (data not shown), which has also been reported previously (Stathonikos *et al*., 2020). Besides, the surgical staff was reduced to minimize potential exposure to infection, and many patients were also reluctant to seek medical attention during this time (Dinmohamed *et al*., 2020). Even though our centre was located in one of the hardest-hit early hotspots in Germany, the number of positive cases was still very low compared with the pandemic activity in some other countries. Therefore, our results cannot be generalized to other centres, countries or pandemic situations. Another limitation includes the use of FFPE material itself. Formalin is known to result in RNA degradation, which might reduce the sensitivity. However, in positive cases, SARS-CoV-2 RNA was detectable even at higher dilutions, when RNA concentration was not detectable or the RNA was strongly degraded, e.g. in autopsy cases.

Finally, our assay approach was not quantitative in terms of viral RNA copy numbers. Accurate quantification is probably not well possible for these samples given the variability in the preanalytical phase and thus potential virus and RNA degradation, i.e. unclear and variable time between surgery/sample collection and formalin fixation and unclear and variable duration of formalin fixation itself. However, from a diagnostic point of view, a dichotomous positive/negative result seems to be sufficient for most applications.

Experimental procedures

Histology samples & cohort description

We routinely analysed diagnostic FFPE samples archived at the Institute of Pathology, University Hospital Aachen. The diagnostic process had been completed for all samples. The study was approved by the local ethics committee (EK 304/20, EK 119/20 and EK 092/20). Details of the total number of identified samples, selection and exclusion criteria, topography of the samples and final numbers of selected samples included into the study are shown in Fig. S3 and outlined in the Supplementary Methods in more detail.

RNA isolation from FFPE specimens and SARS-CoV-2 RNA detection

We extracted RNA from FFPE tissue using a Maxwell® 16 LEV RNA FFPE Purification Kit (Promega GmbH, Walldorf, Germany) on the Maxwell® 16 IVD instrument (Promega GmbH) or with the ReliaPrep™ FFPE Total

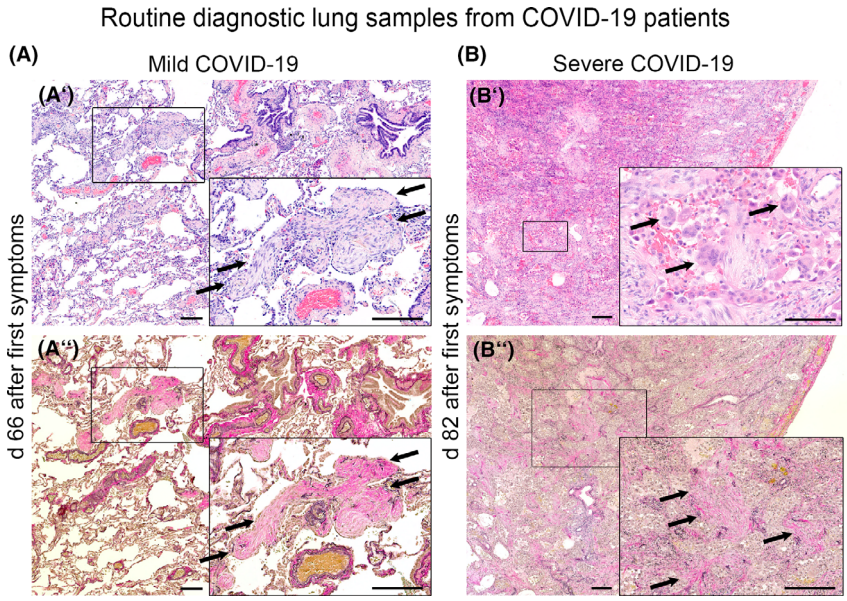

Fig. 3. Histological findings in lungs from patients in the late phase of COVID-19.
A. Histologic images of lung tissue from a patient with lung surgery for pulmonary metastases who had recovered from mild COVID-19 (i.e. without the need for mechanical ventilation), 66 days after initial symptoms. Note the circumscribed fibrotic areas surrounded by thin alveolar septa with open alveolar spaces (arrows, A' hematoxylin-eosin, A'' Elastica van Gieson stain, scale bar = 200 μm).
B. Histological images of lung tissue from a patient with severe COVID-19 (i.e. impaired oxygenation and subsequent failure of mechanical ventilation with the need for extracorporeal membrane oxygenation (ECMO)) with bacterial superinfection. The patient underwent surgery on day 82 after initial symptoms for histologic evaluation of fibrotic changes in the lungs. Note disappeared macrophage-filled alveolar spaces and multinucleated giant cells (B' arrows, hematoxylin–eosin, scale bar = 250 μm, insert: scale bar = 100 μm) and diffusely fibrotic alveolar septa (B'') arrows, Elastica van Gieson stain, scale bar = 250 μm, insert: scale bar = 250 μm.

RNA Miniprep System (Promega GmbH) according to the manufacturer's instructions. The workflow for sample preparation is shown in Fig. S2. We stored the RNA samples at −80°C until further processing.

We examined two different kits for RT-PCR analysis. We used the TaqMan™ Fast 1-Step Master Mix (Thermo Fisher Scientific GmbH, Dreieich, Germany) for the qualitative detection of the E gene, the RdRp gene (encoding the RNA-dependent RNA polymerase gene) and the N gene (nucleocapsid protein gene) by primer and probe sets labelled with fluorescent reporters and Quencher dyes. We used TaqMan® Exogenous Internal Positive Control reagents (Thermo Fisher Scientific GmbH, Dreieich, Germany) as internal PCR controls. We tested for TaqMan™ singleplex and multiplex assays. RT-PCR was performed according to a previous publication (Remmelink *et al*., 2020). In addition, we used the RealStar® SARS-CoV-2 RT-PCR Kit 1.0 (Altona Diagnostics GmbH, Hamburg, Germany) for qualitative multiplex detection of the S gene (encoding spike glycoprotein) of SARS-CoV-2 and the E gene (encoding envelope protein) of lineage B beta-coronavirus (B-βCoV) using probes labelled with fluorescent reporters and quencher dyes. Internal control was included in the master mix as a PCR inhibition control. RT-PCR was performed according to the manufacturer's instructions (Lohse *et al*., 2020; Visseaux *et al*., 2020). The primer and probe sequences used and the corresponding concentrations for RT-PCR are listed in Table S5.

Evaluation of SARS-CoV-2 RNA detection by SARS-CoV-2 RNA standard

We evaluated the two RT-PCR kits and the different primer and probe sets with the Amplirun® SARS-CoV-2 RNA standard (bestbion dx GmbH, Cologne, Germany) provided with 14 000 viral RNA copies μl^{-1}. We prepared a twofold dilution series with 13 concentrations and measured each concentration as five replicates. We tested the singleplex approach of the TaqMan™ kit with each of the E, RdRp and N genes, the multiplex approach of the TaqMan™ kit with the E and RdRp genes and the multiplex approach of the RealStar® kit, in combination. To further evaluate the methods, we used diluted RNA isolated from FFPE tissue from clinically confirmed COVID-19-positive autopsies (lung and trachea).

Fluorescence in situ *hybridization (FISH)*

We deparaffinized freshly cut 1-μm-thick paraffin sections from the RT-PCR-positive cytology sample and a

clinically confirmed COVID-19-positive autopsy lung sample, followed by dehydration with 100% ethanol. We performed FISH on the sections using the RNAscope® Multiplex Fluorescent Reagent Kit v2 assay (Advanced Cell Diagnostics, Hayward, CA, USA) according to the manufacturer's instructions.

Statistical and data analysis

Using a SARS-CoV-2 RNA standard, we created a twofold dilution series to determine a standard curve for each RT-PCR assay by linear regression of the measured C_t values ($n = 5$) as a function of the logarithmic viral copy number with standard deviation (Fig. S4). We used the linear regression of the established SARS-CoV-2 RNA standard for the target E gene to determine the viral copy number μl^{-1} in unknown samples (Fig. S4). We determined the limit of detection (LOD) of each RT-PCR assay based on the linearity of the twofold dilution series of the SARS-CoV-2 RNA standard by a 95% confidence interval (Forootan *et al*., 2017). Using the slope, we calculated the RT-PCR efficiency E according to the equation $E = 100\times(-1 + 10^{-1/\text{slope}})$ (Vogels *et al*., 2020).

Acknowledgments

The excellent technical help of Inge Losen and Cherelle Timm is gratefully acknowledged.

Author contributions

SVS, ED and PB designed and oversaw the study. SVS, SV and PB wrote the initial draft of the manuscript. SVS, RDB and SV assembled the cohort and collected material. SV carried out RNA extraction and RT-PCR experiments. SVS and RDB carried out histological analyses. PB had the conceptual idea, outlined and financed the study. All authors read and approved the final version of the article.

Conflict of interest

The authors declare that there is nothing to disclose.

References

Afzal, A. (2020) Molecular diagnostic technologies for COVID-19: limitations and challenges. *J Adv Res* **26:** 149–159.

Alexandersen, S., Chamings, A., and Bhatta, T.R. (2020) SARS-CoV-2 genomic and subgenomic RNAs in diagnostic samples are not an indicator of active replication. *Nat Commun* **11:** 6059.

Azzi, L., Carcano, G., Gianfagna, F., Grossi, P., Gasperina, D.D., Genoni, A., *et al*. (2020) Saliva is a reliable tool to detect SARS-CoV-2. *J Infect* **81:** e45–e50.

Best Rocha, A., Stroberg, E., Barton, L.M., Duval, E.J., Mukhopadhyay, S., Yarid, N., *et al*. (2020) Detection of SARS-CoV-2 in formalin-fixed paraffin-embedded tissue sections using commercially available reagents. *Lab Invest* **100:** 1485–1489.

Borczuk, A.C., Salvatore, S.P., Seshan, S.V., Patel, S.S., Bussel, J.B., Mostyka, M., *et al*. (2020) COVID-19 pulmonary pathology: a multi-institutional autopsy cohort from Italy and New York City. *Mod Pathol* **33:** 2156–2168.

Corman, V.M., Landt, O., Kaiser, M., Molenkamp, R., Meijer, A., Chu, D.K.W., *et al*. (2020) Detection of 2019 novel coronavirus (2019-nCoV) by real-time RT-PCR. *Euro Surveill* **25:** 1–8.

Deslandes, A., Berti, V., Tandjaoui-Lambotte, Y., Alloui, C., Carbonnelle, E., Zahar, J.r., *et al*. (2020) SARS-CoV-2 was already spreading in France in late December 2019. *Int J Antimicrob Agents* **55:** 106006.

Dinmohamed, A.G., Visser, O., Verhoeven, R.H.A., Louwman, M.W.J., van Nederveen, F.H., Willems, S.M., *et al*. (2020) Fewer cancer diagnoses during the COVID-19 epidemic in the Netherlands. *Lancet Oncol* **21:** 750–751.

Escher, F., Pietsch, H., Aleshcheva, G., Bock, T., Baumeier, C., Elsaesser, A., *et al*. (2020) Detection of viral SARS-CoV-2 genomes and histopathological changes in endomyocardial biopsies. *ESC Heart Fail* **7:** 2440–2447.

Forootan, A., Sjoback, R., Bjorkman, J., Sjogreen, B., Linz, L., and Kubista, M. (2017) Methods to determine limit of detection and limit of quantification in quantitative real-time PCR (qPCR). *Biomol Detect Quantif* **12:** 1–6.

Guerini-Rocco, E., Taormina, S.V., Vacirca, D., Ranghiero, A., Rappa, A., Fumagalli, C., *et al*. (2020) SARS-CoV-2 detection in formalin-fixed paraffin-embedded tissue specimens from surgical resection of tongue squamous cell carcinoma. *J Clin Pathol* **73:** 754–757.

Hou, Y.J., Okuda, K., Edwards, C.E., Martinez, D.R., Asakura, T., Dinnon, K.H., *et al*. (2020) SARS-CoV-2 reverse genetics reveals a variable infection gradient in the respiratory tract. *Cell* **182(429–446):** e414.

Kim, D., Lee, J.Y., Yang, J.S., Kim, J.W., Kim, V.N., and Chang, H. (2020) The Architecture of SARS-CoV-2 transcriptome. *Cell* **181:** 914–921.e10.

Lamers, M.M., Beumer, J., van der Vaart, J., Knoops, K., Puschhof, J., Breugem, T.I., *et al*. (2020) SARS-CoV-2 productively infects human gut enterocytes. *Science* **369:** 50–54.

Lean, F.Z.X., Lamers, M.M., Smith, S.P., Shipley, R., Schipper, D., Temperton, N., *et al*. (2020) Development of immunohistochemistry and in situ hybridisation for the detection of SARS-CoV and SARS-CoV-2 in formalin-fixed paraffin-embedded specimens. *Sci Rep* **10:** 21894.

Lescure, F.-X., Bouadma, L., Nguyen, D., Parisey, M., Wicky, P.-H., Behillil, S., *et al*. (2020) Clinical and virological data of the first cases of COVID-19 in Europe: a case series. *Lancet Infect Dis* **20:** 697–706.

Liu, J., Babka, A.M., Kearney, B.J., Radoshitzky, S.R., Kuhn, J.H., and Zeng, X. (2020) Molecular detection of SARS-CoV-2 in formalin-fixed, paraffin-embedded specimens. *JCI Insight* **5:** 1–7.

Lodder, W., and de Roda Husman, A.M. (2020) SARS-CoV-2 in wastewater: potential health risk, but also data source. *Lancet Gastroenterol Hepatol* **5:** 533–534.

Lohse, S., Pfuhl, T., Berkó-Göttel, B., Rissland, J., Geißler, T., Gärtner, B., *et al*. (2020) Pooling of samples for testing for SARS-CoV-2 in asymptomatic people. *Lancet Infect Dis* **20:** 1231–1232.

Mei, F., Bonifazi, M., Menzo, S., Di Marco Berardino, A., Sediari, M., Paolini, L., *et al*. (2020) First detection of SARS-CoV-2 by Real-Time Reverse Transcriptase-polymerase chain reaction assay in pleural fluid. *Chest* **158:** e143–e146.

Menter, T., Haslbauer, J.D., Nienhold, R., Savic, S., Hopfer, H., Deigendesch, N., *et al*. (2020) Postmortem examination of COVID-19 patients reveals diffuse alveolar damage with severe capillary congestion and variegated findings in lungs and other organs suggesting vascular dysfunction. *Histopathology* **77:** 198–209.

Oran, D.P., and Topol, E.J. (2020) Prevalence of asymptomatic SARS-CoV-2 infection: a narrative review. *Ann Intern Med* **173:** 362–367.

Polak, S.B., Van Gool, I.C., Cohen, D., von der Thusen, J.H., and van Paassen, J. (2020) A systematic review of pathological findings in COVID-19: a pathophysiological timeline and possible mechanisms of disease progression. *Mod Pathol* **33:** 2128–2138.

Puelles, V.G., Lütgehetmann, M., Lindenmeyer, M.T., Sperhake, J.P., Wong, M.N., Allweiss, L., *et al*. (2020) Multiorgan and renal tropism of SARS-CoV-2. *N Engl J Med* **383:** 590–592.

Remmelink, M., De Mendonça, R., D'Haene, N., De Clercq, S., Verocq, C., Lebrun, L., *et al*. (2020) Unspecific post-mortem findings despite multiorgan viral spread in COVID-19 patients. *Crit Care* **24:** 495.

Sekulic, M., Harper, H., Nezami, B.G., Shen, D.L., Sekulic, S.P., Koeth, A.T., *et al*. (2020) Molecular Detection of SARS-CoV-2 infection in FFPE samples and histopathologic findings in fatal SARS-CoV-2 cases. *Am J Clin Pathol* **154:** 190–200.

Smithgall, M.C., Liu-Jarin, X., Hamele-Bena, D., Cimic, A., Mourad, M., Debelenko, L., and Chen, X. (2020) Third-trimester placentas of severe acute respiratory syndrome coronavirus 2 (SARS-CoV-2)-positive women: histomorphology, including viral immunohistochemistry and in-situ hybridization. *Histopathology* **77:** 994–999.

Stathonikos, N., van Varsseveld, N.C., Vink, A., van Dijk, M.R., Nguyen, T.Q., Leng, W.W.J.d., *et al*. (2020) Digital pathology in the time of corona. *J Clin Pathol* **73:** 706–712.

von Stillfried, S., and Boor, P. (2021) Methods of SARS-CoV-2 detection in tissue. *Pathologe* **42(2):** 208–215. https://10.1007/s00292-021-00920-1.

von Stillfried, S., Bulow, R.D., Rohrig, R., Knuchel-Clarke, R., Boor, P., and DeRegCovid (2020) Autopsy registry can facilitate COVID-19 research. *EMBO Mol Med* **12:** e12885.

Streeck, H., Schulte, B., Kümmerer, B.M., Richter, E., Höller, T., Fuhrmann, C., *et al*. (2020) Infection fatality rate of SARS-CoV2 in a super-spreading event in Germany. *Nat Commun* **11:** 5829.

Taylor, S., Wakem, M., Dijkman, G., Alsarraj, M., and Nguyen, M. (2010) A practical approach to RT-qPCR-Publishing data that conform to the MIQE guidelines. *Methods* **50:** S1–5.

Visseaux, B., Le Hingrat, Q., Collin, G., Ferre, V., Storto, A., Ichou, H., *et al*. (2020) Evaluation of the RealStar(R) SARS-CoV-2 RT-PCR kit RUO performances and limit of detection. *J Clin Virol* **129:** 104520.

Vogels, C.B.F., Brito, A.F., Wyllie, A.L., Fauver, J.R., Ott, I.M., Kalinich, C.C., *et al*. (2020) Analytical sensitivity and efficiency comparisons of SARS-CoV-2 RT-qPCR primer-probe sets. *Nat Microbiol* **5:** 1299–1305.

Wang, D., Hu, B.o., Hu, C., Zhu, F., Liu, X., Zhang, J., *et al*. (2020) Clinical Characteristics of 138 HOSPITALIZED PATIENTS WITH 2019 Novel Coronavirus-infected pneumonia in Wuhan. *China, JAMA* **323:** 1061–1069.

Wichmann, D., Sperhake, J.P., Lutgehetmann, M., Steurer, S., Edler, C., Heinemann, A., *et al*. (2020) Autopsy findings and venous thromboembolism in patients With COVID-19: a prospective cohort study. *Ann Intern Med* **173:** 268–277.

Supporting information

Additional supporting information may be found online in the Supporting Information section at the end of the article.

Fig. S1. Comparison of two RNA isolation systems (Promega vs. Zymo Research) using clinically confirmed COVID-19 autopsy tissues by total RNA yield (a), quality (b, c) and RT-PCR results in samples with (d) high (Patient No. 1–4) and (e) low viral load (Patient No. 5–8).

Fig. S2. Workflow for RNA isolation from FFPE specimens and SARS-CoV-2 RNA detection using RT-PCR. (a) RNA extraction. (b) RT-PCR amplification protocol used. (c) Interpretation of RT-PCR results.

Fig. S3. Flow chart of sample selection of patients' cohorts After identifying all eligible samples, we excluded cases without the availability of FFPE material in all cohorts. Next, we excluded cases from locations other than the predefined localizations in the peak pandemic cohort and the pre-pandemic cohort. Finally, we excluded FFPE samples with low tissue quantity or quality in all cohorts.

Fig. S4. Linear Regression and data analysis of the various RT-PCR methods. Determination of slope, y-intercept, R2 and RT-PCR efficiency by five replicates of 2-fold dilution series of the SARS-CoV-2 RNA standard of the approaches TaqMan singleplex (E, RdRp and N gene), TaqMan multiplex (E, RdRp gene) and RealStar multiplex (S gene and B-ßCoV E gene).

Table S1. Sample characteristics for COVID-19 Patients Cohort.

Table S2. Sample characteristics for the Pandemic Peak Cohort.

Table S3. Detailed topography of samples from the Pandemic Peak Cohort.

Table S4. Sample characteristics for Pre-pandemic Cohort.

Table S5. Primer and probe set overview used in TaqMan and RealStar RT-PCR method.

